

# 修士学位論文

Developing a High Resolution  
Communication System Utilizing High  
Frequency Bands for Beyond 5G

Beyond 5G に対応した高周波数帯のネット  
ワーク構築を実現するためのフレキシブル  
な5Gセンサーとアンテナの構築

2023年1月6日提出  
総合分析情報学コース  
指導教員 中尾彰宏 教授  
49-216421  
三谷 恵司

# Contents

<b>1</b>	<b>Introduction</b>	<b>1</b>
1.1	Background . . . . .	1
1.2	Problem Statement . . . . .	1
1.3	Thesis Statement . . . . .	2
1.4	Related Work . . . . .	2
1.5	Contributions . . . . .	2
1.6	Organization . . . . .	2
1.7	Security . . . . .	2
1.7.1	TEMPEST Attack . . . . .	2
1.7.2	Attacks on omni-directional antennas . . . . .	2
<b>2</b>	<b>Theory of Physical Communication Mediums</b>	<b>4</b>
2.1	Mathematical analysis of waveguides . . . . .	4
2.2	Horn Antennas . . . . .	7
2.3	Radar . . . . .	10
2.4	Antenna Gain . . . . .	10
2.5	Antenna Impedance . . . . .	10
2.5.1	Impedance in low frequencies . . . . .	11
2.5.2	Impedance in high frequencies . . . . .	12
2.6	The Friis Equation . . . . .	13
2.7	Loss tangent . . . . .	14
2.8	Skin effect . . . . .	16
2.9	Snell's law . . . . .	16
2.10	Total Reflection . . . . .	17
2.11	Link budget . . . . .	18
2.12	S parameters . . . . .	19
2.13	Cutoff Frequency . . . . .	19
2.14	Usecases . . . . .	20
2.15	Two Dimensional Waveguide Sheets . . . . .	21
2.16	Finite Element Boundary Integral Method . . . . .	21
2.16.1	Boundary Integral Equation Methods . . . . .	21
2.17	Radiation Conditions . . . . .	22

## CONTENTS

---

2.18 Huygens' principle . . . . .	22
2.19 Variational Method . . . . .	22
2.19.1 The Ritz Method . . . . .	23
2.19.2 Galerkin's Method . . . . .	24
2.19.3 A Simple example . . . . .	24
2.20 Summary . . . . .	25
2.21 Rod Antennas . . . . .	26
2.22 Tools to Use . . . . .	26
2.22.1 Vector network analyzers . . . . .	26
2.22.2 Connectors . . . . .	26
2.22.3 MZ-mmCon1 . . . . .	26
2.22.4 MZ-mmAnt1 . . . . .	26
2.22.5 Shield Box . . . . .	26
2.22.6 Adalm Pluto . . . . .	29
2.22.7 Waveguide to Coax Adapter . . . . .	29
2.22.8 Spectrum Analyzer . . . . .	29
2.23 Communication Medium Used in Embedded Systems . . . . .	29
2.23.1 UART . . . . .	29
2.23.2 SPI . . . . .	31
2.24 Grating Couplers . . . . .	32
2.25 Luneburg Lens . . . . .	32
2.25.1 Uses in a microwave antenna . . . . .	33
2.26 Qualitative Analysis . . . . .	33
2.27 Quantitative Analysis . . . . .	34
2.27.1 Spectrum Results . . . . .	34
2.27.2 Directivity Results . . . . .	34
<b>3 PTFE Rod Antenna</b>	<b>37</b>
3.1 PTFE Rod Antenna Realization . . . . .	37
3.2 Simulation Using HFSS . . . . .	37
3.2.1 About the simulation conditions . . . . .	37
3.2.2 About the models . . . . .	37
<b>4 Conclusion</b>	<b>40</b>
<b>5 Future Work</b>	<b>41</b>
<b>Bibliography</b>	<b>42</b>

# List of Figures

2.1	Model of metal waveguide . . . . .	5
2.2	Geometry of metal waveguide . . . . .	8
2.3	Cross section of waveguide, cut in the H-plane . . . . .	8
2.4	Cross section of waveguide, cut in the E-plane . . . . .	9
2.5	Model of horn antenna . . . . .	9
2.6	Circuit model of antenna connected to voltage source . . . . .	11
2.7	High frequency circuit model . . . . .	12
2.8	Transmit (Tx) and Receive (Rx) Antennas separated by R . . . . .	13
2.9	Comparison of Loss with Different Frequencies . . . . .	15
2.10	Evanescence waves present in total internal reflection . . . . .	18
2.11	MZ-mmcon1 in loopback mode . . . . .	27
2.12	Adalm Pluto . . . . .	27
2.13	FFT visualization on the software . . . . .	27
2.14	mz-mmAnt1 . . . . .	28
2.15	Waveguide to Coax Adapter . . . . .	28
2.16	Shield Box . . . . .	28
2.17	VR-WH1 placed inside shield box . . . . .	28
2.18	Conversion of the port on MS2762A . . . . .	30
2.19	The mz-mmAnt1 hooked up to the MS2762A . . . . .	30
2.20	UART with data bus . . . . .	31
2.21	UART packet . . . . .	31
2.22	SPI Communication . . . . .	32
2.23	Luneburg lens . . . . .	33
2.24	Video does not play (data is not received) when the waveguide is not pointed to the receiver . . . . .	34
2.25	Video plays when the waveguide is pointed to the receiver . . . . .	34
2.26	PTFE rod antenna with a diameter of 10 mm and length of 20 cm . . . . .	35
2.27	Placement of antenna in anechoic chamber . . . . .	35
2.28	PTFE rod antenna in anechoic chamber . . . . .	35
2.29	Horn antenna in anechoic chamber . . . . .	35
2.30	Vertical Radiation Pattern . . . . .	36
2.31	Horizontal Radiation Pattern . . . . .	36

## LIST OF FIGURES

---

3.1	Solution Type for HFSS . . . . .	38
3.2	Region Specification for HFSS . . . . .	38
3.3	Waveport Models for HFSS . . . . .	38
3.4	Solution Setup for HFSS . . . . .	38
3.5	Integration Line for HFSS . . . . .	39
3.6	Integration Line for HFSS for HFSS . . . . .	39

# List of Tables

2.1	Comparisons of Preferred Gain . . . . .	10
2.2	Table of all factors affecting the communication system . . . . .	19

# Chapter 1

## Introduction

### 1.1 Background

The fifth generation (5G) mobile communication system is expected to provide new innovations to support the society with technical features including high speed, high capacity, low latency, and massive connectivity. As a special feature of 5G, high frequency bands such as the millimeter wave bands are supported to achieve ultra-high speed wireless data communications of several gigabits per second using a frequency bandwidth of several-hundred megahertz [1].

### 1.2 Problem Statement

Millimeter wave 5G technology can provide massive capacity and even lower latency than previous technologies such as 4G. However, millimeter waves also have problems and limitations that need to be addressed:

**Performance degradation in NLOS environments** Propagation losses in line-of sight (LOS), where the path between the device and the base station is unobstructed, and performance degradation in non-line-of-sight (NLOS), where the path is blocked, environments are crucial issues for mobile communication systems in the millimeter wave bands. As the received power on the device decreases, the communication area becomes much smaller than when utilizing lower frequency bands.

**High directivity** Due to the high directivity of millimeter waves, solutions such as beamforming and beam steering techniques employing array antenna systems are necessary to mitigate these issues. These technologies are already implemented in 5G base station tools. [2]

**Short propagation distance** Due to its high frequency, millimeter waves have high propagation loss, and can only travel short distances.

TODO: add LOS and NLOS images

## 1.3 Thesis Statement

In order to efficiently solve the problems mentioned above, we propose to design a high resolution communication system using dielectric materials. TODO: write more

## 1.4 Related Work

Dielectric materials have been used as antennas for some time. In millimeter wave bands, Kawai et al. have proposed an approach that expands communication areas by using a flexible dielectric waveguide, which has low loss characteristics in the millimeter wave band range [3]. Fukuda et al. have proposed a leaky-wave antenna employing a bent dielectric waveguide for millimeter wave bands [4]. The study utilizes the characteristics that the dielectric waveguide radiates electromagnetic waves by inflection, and that the inflected part of the waveguide acts as an antenna. Since the inflected part can be formed anywhere along the length of the waveguide, it is possible to expand communication areas around the waveguide. Antenna gain values of 3 dB to 5 dB are achieved in both H-plane and V-plane, and a narrow beam was created in the V-plane. TODO

## 1.5 Contributions

Compared to existing work and communication mediums, the designed dielectric antenna can ... TODO

## 1.6 Organization

This paper designs a high resolution PTFE rod antenna and details the design and implementation process.

The thesis chapters are organized as follows.

## 1.7 Security

### 1.7.1 TEMPEST Attack

The TEMPEST attack is used to eavesdrop on leaked electromagnetic radiation that can directly provide plaintexts and other information. Leaked electromagnetic radiation can have a variety of sources, from cables, laptop computers, and antennas.

### 1.7.2 Attacks on omni-directional antennas

We look at an example of omni-directional antennas being attacked. In a hostile environment, the adversary's antenna can pick up signals from the transmitter when the SNR at

## 1.7. SECURITY

the antenna of the adversary is high enough. In case of an omni-directional antenna, it can have a coverage of 360 degrees and send data in all directions horizontally. This can be both a waste of power and network capacity, and can allow hostile devices to detect the radiated signals [5]. Therefore, using directive antennas, which form directional beams towards the receiver, can be considered to be more safe.

# Chapter 2

## Theory of Physical Communication Mediums

### 2.1 Mathematical analysis of waveguides

Waveguides are devices for transporting electromagnetic energy from one region to another. There are a variety of waveguides, from hollow tubes made out of metal to sticks made of teflon. First we analyze waveguides that are hollow metal tubes (often rectangular or circular in cross section). These waveguides are capable of directing power precisely to where it is needed, can handle large amounts of power and function as a high-pass filter.

Here we examine metal waveguides with a rectangular cross section. In a source-free region, it is known that

$$\nabla D = 0 \quad (2.1)$$

where  $D$  is the electric flux density. If a vector quantity is divergenceless, then it can be expressed as the curl of another quantity. The solution for  $D$  and the corresponding electric field  $E$  can be written as:

$$D = -\nabla \times F \quad (2.2)$$

$$E = \frac{-1}{\epsilon} \nabla \times F \quad (2.3)$$

where  $\epsilon$  is the permittivity of the medium where the wave propagates. Here for simplicity, it is assumed that  $E_z$  is zero. The following equations describing the electric and magnetic fields can be derived from Maxwell's equations.

$$E_x = -\frac{1}{\epsilon} \frac{\partial F_z}{\partial y} \quad (2.4)$$

## 2.1. MATHEMATICAL ANALYSIS OF WAVEGUIDES

---

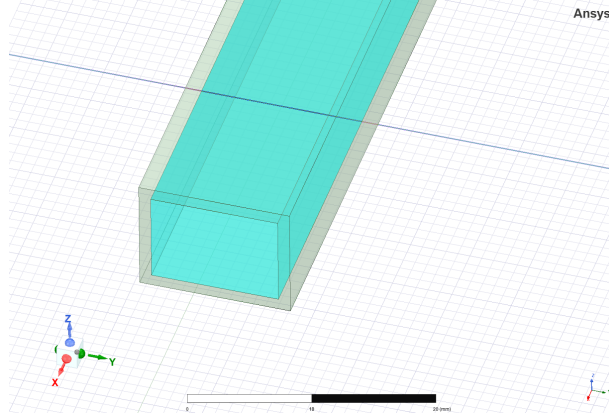


Fig. 2.1: Model of metal waveguide

$$E_y = \frac{1}{\epsilon} \frac{\partial F_z}{\partial x} \quad (2.5)$$

$$E_z = 0 \quad (2.6)$$

$$H_x = -j \frac{1}{\omega \mu \epsilon} \frac{\partial^2 F_z}{\partial x \partial z} \quad (2.7)$$

$$H_y = -j \frac{1}{\omega \mu \epsilon} \frac{\partial^2 F_z}{\partial y \partial z} \quad (2.8)$$

$$H_z = -j \frac{1}{\omega \mu \epsilon} \left( \frac{\partial^2}{\partial z^2} + k^2 \right) F_z \quad (2.9)$$

Here,  $k$  is the wave number. If the  $F_z$ , which is the z-axis component of the vector  $F$ , is found, then the electric and magnetic fields can be found. From Maxwell's equations, the vector potential  $F$  must satisfy the vector wave equation in a source-free region.

$$\left( \nabla^2 - \frac{1}{c^2} \frac{\partial^2}{\partial t^2} \right) \mathbf{F} = 0 \quad (2.10)$$

Assuming that there is only one frequency, the time dependence can be written as

$$e^{j\omega t} = e^{j2\pi f t} \quad (2.11)$$

Thus, the equation [2.10] can be rewritten as follows:

$$\nabla^2 F_z + k^2 F_z = 0 \quad (2.12)$$

The technique of separation of variables is used to solve this equation. It can be assumed that  $F_z$  can be separated into the product of 3 functions.

$$F_z(x, y, z) = X(x)Y(y)Z(z) \quad (2.13)$$

Therefore, when equation [2.13] is plugged into equation [2.12], the following equation is derived (the prime represents the derivative):

$$\frac{X''}{X} + \frac{Y''}{Y} + \frac{Z''}{Z} = -k^2 \quad (2.14)$$

For simplicity, the wavenumber  $k$  will be broken into components as below:

$$k^2 = k_x^2 + k_y^2 + k_z^2 \quad (2.15)$$

Using equation [2.15] and the fact that all variables are independent in equation [2.14], the following ordinary differential equations are derived:

$$\begin{cases} X'' + k_x^2 X = 0 \\ Y'' + k_y^2 Y = 0 \\ Z'' + k_z^2 Z = 0 \end{cases} \quad (2.16)$$

Solving the above equations, we get:

$$\begin{cases} X(x) = c_1 \cos(k_x x) + c_2 \sin(k_x x) \\ Y(y) = c_3 \cos(k_y y) + c_4 \sin(k_y y) \\ Z(z) = c_5 e^{jk_z z} + c_6 e^{-jk_z z} \end{cases} \quad (2.17)$$

The variable  $c_5$  can be eliminated as 0, since waves analyzed here are propagating in the  $+z$  direction. Plugging in the solutions above,  $F_z$  can be written as

$$F_z = [c_1 \cos(k_x x) + c_2 \sin(k_x x)][c_3 \cos(k_y y) + c_4 \sin(k_y y)]c_6 e^{-jk_z z} \quad (2.18)$$

Using the condition that tangential electric fields in perfect conductors must be zero,  $E_x$  must be zero when  $y = 0$  and  $y = b$ . The same could be said for  $E_y$ , which is also zero when  $x = 0$  and  $x = a$ .  $E_x$  can be calculated as:

$$\begin{aligned} E_x &= -\frac{1}{\epsilon} \frac{\partial F_z}{\partial y} \\ &= -\frac{c_6 k_y}{\epsilon} [c_1 \cos(k_x x) + c_2 \sin(k_x x)][-c_3 \sin(k_y y) + c_4 \cos(k_y y)]e^{-jk_z z} \end{aligned} \quad (2.19)$$

The boundary condition for  $E_x$  is given by:

$$E_x(x, y = 0, z) = 0 \quad (2.20)$$

This implies that  $c_4$  must be equal to zero. As for the second boundary condition,

$$E_x(x, y = b, z) = 0 \quad (2.21)$$

## 2.2. HORN ANTENNAS

---

This means that  $c_3 \sin(k_y b) = 0$ , which means that the wavenumber  $k_y$  can be written as follows:

$$k_y = \frac{n\pi}{b} \quad (2.22)$$

$n$  here is a natural number. This states that the only solutions for  $Y(y)$  function must be sinusoids, and must have a wavenumber which consists an integer number of multiples of a half-wavelength. Simiarly in the y-axis, the following can be derived:

$$k_x = \frac{m\pi}{a} \quad (2.23)$$

This statement implies that the only functions of x that satisfy the differential equation and the required boundary conditions must be an integer multiple of half-sinusoids within the waveguide. Combining these results, the solution for  $F_z$  can be written as

$$\begin{aligned} F_z &= A \cos(k_x x) \cos(k_y y) \exp(-jk_z z) \\ &= A \cos\left(\frac{m\pi x}{a}\right) \cos\left(\frac{n\pi y}{b}\right) \exp(-jk_z z) \end{aligned} \quad (2.24)$$

Only certain distributions will satisfy the required differential equations and the boundary conditions. These configurations are called modes. Since this solution assumed that  $E_z$  is zero, this mode is written as the  $TE_{mn}$  mode.

Due to Maxwell's Equations, the fields within the waveguide always have a specific "form" or "waveshape", which are known as modes. Assume the waveguide is oriented such that the energy is to be transmitted along the waveguide axis, the z-axis. The modes are classified as either TE ('transverse electric' - which indicates that the E-field is orthogonal to the axis of the waveguide, so that  $E_z=0$ ) or TM ('transverse magnetic' - which indicates that the H-field is orthogonal to the axis of the waveguide, so  $H_z = 0$ ). The modes are further classified as  $TE_{ij}$ , where the  $i$  and  $j$  indicate the number of wave oscillations for a particular field direction in the long direction (dimension  $a$  in Figure 2.2) and short direction (dimension  $b$  in Figure 2.2), respectively. Metal waveguides cannot support the TEM ('transverse electric and magnetic' - when  $E_z$  and  $H_z$  are zero) mode. Their exists no solution to Maxwell's equations that also satisfy the required boundary conditions for this mode to occur.

TODO: add from here <https://www.antenna-theory.com/tutorial/waveguides/waveguides3.php>

## 2.2 Horn Antennas

Horn antennas are used in high frequency bands spanning from 300MHz to even as high as 100GHz. Horn antennas often have a directional radiation pattern with a high antenna gain, which can range up to 25 dB in some cases, with 10-20 dB being typical. Horn antennas have a wide impedance bandwidth, implying that the input impedance is slowly varying over a wide frequency range (which also implies low values for S11 or VSWR).

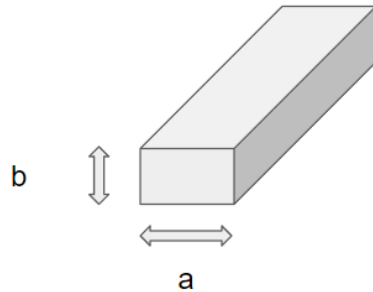


Fig. 2.2: Geometry of metal waveguide

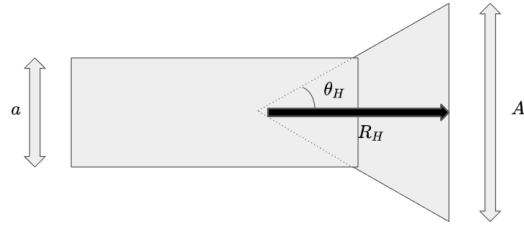


Fig. 2.3: Cross section of waveguide, cut in the H-plane

The bandwidth for practical horn antennas can be on the order of 20:1 (for instance, operating from 1 GHz-20 GHz), with a 10:1 bandwidth not being uncommon.

The E-field in the far-field becomes linearly polarized. The magnitude of the E-field can be written as:

$$|E| = \frac{k}{4\pi r} (1 + \cos(\theta)) \int_{-B/2}^{B/2} \int_{-A/2}^{A/2} E_A(x, y) e^{jk(x \sin \theta \cos \phi + y \sin \theta \sin \phi)} dx dy \quad (2.25)$$

This equation implies that the far-fields of the horn antenna is the Fourier Transform of the fields at the opening of the horn.

TODO: copy here <https://www.thefouriertransform.com/applications/radiation.php>  
Modeling the electric field as the magnetic surface current  $M_S$ , it can be written as:

$$M_S = E_a \times \hat{n} \quad (2.26)$$

## 2.2. HORN ANTENNAS

---

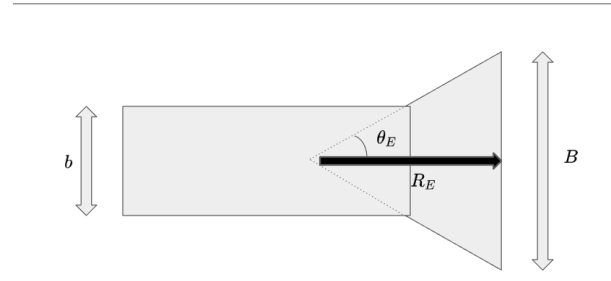


Fig. 2.4: Cross section of waveguide, cut in the E-plane

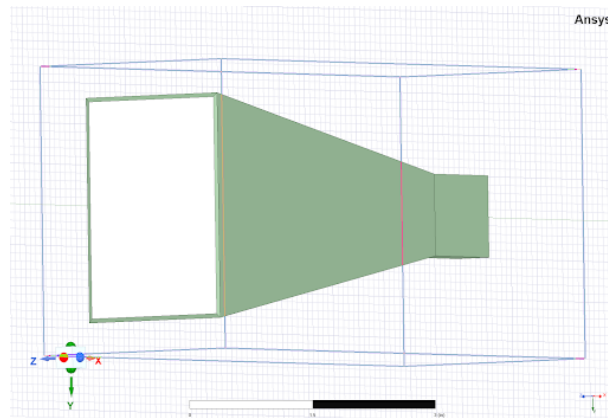


Fig. 2.5: Model of horn antenna

$\hat{n}$  is the unit vector perpendicular to the surface. The electric fields  $E$  and magnetic fields  $H$  in the far field can be written as:

$$E = \eta H \times \hat{r} \quad (2.27)$$

$$H = \hat{r} \times \frac{E}{\eta} \quad (2.28)$$

Here,  $\eta$  is the characteristic impedance of free space, which is about 377 Ohms.  $\hat{r}$  is the direction of propagation for the plane wave.

The waveguide feed acts as a high-pass filter, which blocks any energy below its cutoff frequency. The antenna gain is affected by the geometry of the horn antenna.

## 2.3 Radar

Radar works by transmitting an electromagnetic wave from an antenna. The wave then bounces off some object, and the returned energy is measured. The amount of energy returned is a function of the radar cross section of the object.

If we can estimate the fields radiated by an antenna, we can estimate the surface electric current induced on an object (such as an airplane).

## 2.4 Antenna Gain

The term antenna gain describes how much power is transmitted in the direction of peak radiation to that of an isotropic source. A transmitting antenna with a gain of 3 dB means that the power received far from the antenna will be 3 dB higher (twice as much) than what would be received from a lossless isotropic antenna with the same input power. Note that a lossless antenna would be an antenna with an antenna efficiency of 0 dB. Similarly, a receive antenna with a gain of 3 dB in a particular direction would receive 3 dB more power than a lossless isotropic antenna. Antenna Gain is sometimes discussed as a function of angle. In this case, we are essentially plotting the radiation pattern, where the units (or magnitude of the pattern) are measured in antenna gain. Often manufacturers of antennas (be they wifi antennas, gps antennas, or tv antennas) specify the antenna gain. For instance, manufacturers of wifi antennas may market the wifi antenna as a "high gain antenna", which is more expensive than a similar low gain antenna. Here we discuss how different devices have different gain, as the need for high/low gain differs depends on the situation.

Table 2.1: Comparisons of Preferred Gain

Example	Preferred Gain	Reason
TV antennas	High	Location of the broadcast antennas are known.
GPS	Low	Location of GPS satellites are unknown
Mobile Cellular Antennas	Low	Location of cell towers are unknown

## 2.5 Antenna Impedance

Antenna impedance relates the voltage to the current at the input to the antenna. This is an important parameter to look out for when conducting experiments.

For instance, when an antenna has an impedance of 50 ohms, this means that if a sinusoidal voltage is applied at the antenna terminals with an amplitude of 1 Volt, then the current will have an amplitude of  $1/50 = 0.02$  Amps. Since the impedance is a real number, the voltage is in-phase with the current.

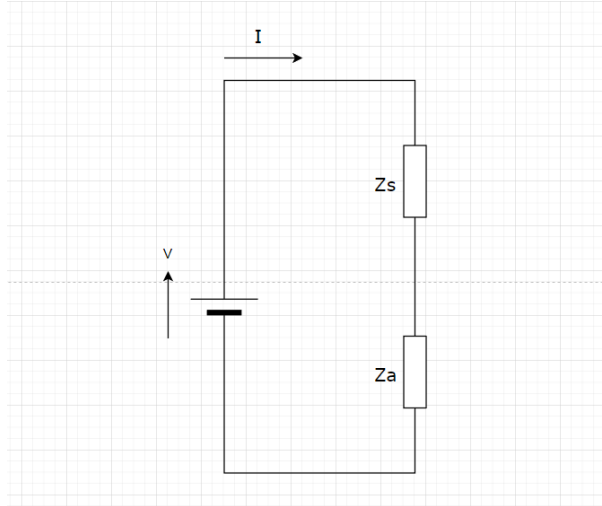


Fig. 2.6: Circuit model of antenna connected to voltage source

Alternatively, when the impedance is given by a complex number, the phase will need to be considered additionally to the amplitude. If impedance  $Z$  is written as  $50 + j * 50$ , where  $j$  is an imaginary number, then the impedance has a magnitude equal to:

$$\sqrt{50^2 + 50^2} = 70.71 \quad (2.29)$$

The phase can be calculated as:

$$\tan^{-1}\left(\frac{\text{Im}(Z)}{\text{Re}(Z)}\right) = \frac{\pi}{4} \quad (2.30)$$

The real part of the antenna impedance represents power that is either radiated away or absorbed within the antenna. The imaginary part of the impedance represents power that is stored in the near field of the antenna. This is non-radiated power. An antenna with a real input impedance (zero imaginary part) is said to be resonant.

### 2.5.1 Impedance in low frequencies

When we are dealing with low frequencies, the transmission line that connects the transmitter or receiver to the antenna is short relative to the wavelength.

Consider an antenna which is represented as an impedance given by  $Z_A$ , hooked up to a voltage source (of magnitude  $V$ ) with source impedance given by  $Z_s$ . The equivalent circuit of this is shown in Figure 2.6.

Using the equation  $P = IV$  from circuit theory, the power delivered to the antenna can be calculated as:

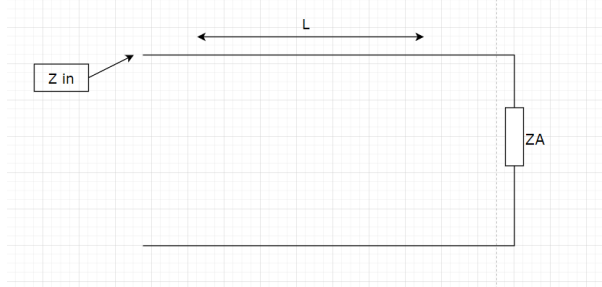


Fig. 2.7: High frequency circuit model

$$P_A = \frac{V^2 Z_A}{(Z_A + Z_S)^2} \quad (2.31)$$

If  $Z_A$  is much smaller in magnitude than  $Z_S$ , then no power will be delivered to the antenna and it won't transmit or receive energy. The same can be said when  $Z_A$  is much larger in magnitude than  $Z_S$ . The ideal value for antenna impedance when maximum power is transferred is given as:

$$Z_A = Z_S^* \quad (2.32)$$

where  $Z_S^*$  is the complex conjugate of  $Z_S$ . For example, if  $Z_S = 30 + 30j$ , then  $Z_A = 30 - 30j$  is the ideal impedance for maximum power transfer.

### 2.5.2 Impedance in high frequencies

In low-frequency circuit theory, the wires that connect things don't matter. Once the wires become a significant fraction of a wavelength, the situation changes. For instance, a short circuit has an impedance of zero ohms. However, if the impedance is measured at the end of a quarter wavelength transmission line, the impedance appears to be infinite, even though there is a direct current conduction path.

In general, the transmission line will transform the impedance of an antenna, making it very difficult to deliver power, unless the antenna is matched to the transmission line. Consider the situation shown in Figure 2.7. The impedance is to be measured at the end of a transmission line (with characteristic impedance  $Z_0$ ) and Length  $L$ . The end of the transmission line is hooked to an antenna with impedance  $Z_A$ .

Input impedance  $Z_{in}$  is given by:

$$Z_{in} = Z_0 \frac{Z_A + jZ_0 \tan(\frac{2\pi f}{c})L}{Z_0 + jZ_A \tan(\frac{2\pi f}{c})L} \quad (2.33)$$

If the antenna is matched to the transmission line ( $Z_A = Z_0$ ), then the input impedance does not depend on the length of the transmission line.

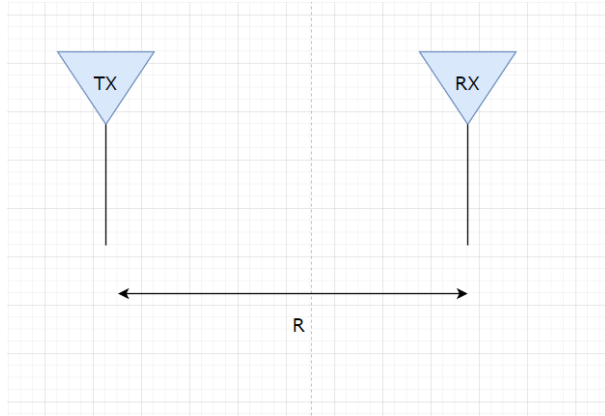


Fig. 2.8: Transmit (Tx) and Receive (Rx) Antennas separated by R.

If the antenna is not matched, the input impedance will vary widely with the length of the transmission line. And if the input impedance isn't well matched to the source impedance, not very much power will be delivered to the antenna. This power ends up being reflected back to the generator, which can be a problem in itself (especially if high power is transmitted). This loss of power is known as impedance mismatch. Hence, having a tuned impedance for an antenna is extremely important.

## 2.6 The Friis Equation

One of the most fundamental equations in antenna theory is the Friis Transmission Equation. The Friis Transmission Equation is used to calculate the power received from one antenna (with gain  $G_1$ ), when transmitted from another antenna (with gain  $G_2$ ), separated by a distance  $R$ , and operating at frequency  $f$  or wavelength  $\lambda$ . The two antennas are considered to be in free space.

Assume that  $P_T$  watts of total power are delivered to the transmit antenna and that the transmit antenna is omnidirectional, lossless, and that the receive antenna is in the far field of the transmit antenna. Then the power density  $p$  (in Watts per square meter) from the transmit antenna is given by:

$$p = \frac{P_T}{4\pi R^2} \quad (2.34)$$

If the transmit antenna has an antenna gain in the direction of the receive antenna given by  $G_T$ , then the power density can be written as:

$$p = \frac{P_T}{4\pi R^2} G_T \quad (2.35)$$

The gain term factors in the directionality and losses of a real antenna. Assume now

## 2.7. LOSS TANGENT

---

that the receive antenna has an effective aperture given by  $A_E R$ . Then the power received by this antenna  $P_R$  is given by:

$$p = \frac{P_T}{4\pi R^2} G_T A_E R \quad (2.36)$$

Since the effective aperture for any antenna can also be expressed as:

$$A_e = \frac{\lambda^2}{4\pi} G \quad (2.37)$$

Plugging in this result, the received power can be rewritten as:

$$p = \frac{P_T G_T G_R \lambda^2}{(4\pi R)^2} \quad (2.38)$$

Equation 2.38 is the Friis Transmission Formula, and relates the free space path loss, antenna gains and wavelength to the received and transmit powers.

When we plug in the wave equation  $c = f\lambda$ , where  $c$  is the speed of light,  $f$  is the frequency, and  $\lambda$  is the wavelength, we get:

$$P_R = \frac{P_T G_T G_R c^2}{(4\pi R f)^2} \quad (2.39)$$

Equation 2.39 shows that more power is lost at higher frequencies. This means that for antennas with specified gains, the energy transfer will be highest at lower frequencies. The difference between the power received and the power transmitted is known as path loss.

Using 2.38, loss  $L$  (in decibels) in free space can be rewritten as follows:

$$L = \left( \frac{4\pi d}{\lambda} \right)^2 \quad (2.40)$$

At 28GHz, which has the wave length of 1 cm, the loss at the distance of 0.25 cm can be computed as -49.3 decibels. At 800MHz (wave length of 37.5 cm), the same loss of -49.3 decibels can be seen at the distance of 10 meters. The comparison of these two frequencies is shown in Figure 2.9.

## 2.7 Loss tangent

In a dielectric material, dielectric loss quantifies the inherent dissipation of electromagnetic energy, and can be parametrized in terms of the loss tangent. The basic equation for electromagnetic waves when there is loss in the medium is as follows

$$\text{rot}\left(\frac{1}{\mu(\mathbf{r})}\text{rot}\mathbf{E}\right) = -\mu_0\text{rot}\left(\frac{\partial H}{\partial t}\right) \quad (2.41)$$

## 2.7. LOSS TANGENT

---



Fig. 2.9: Comparison of Loss with Different Frequencies

$$\text{rot}\left(\frac{\partial H}{\partial t}\right) = \epsilon(\mathbf{r})\epsilon_0 \frac{\partial^2 E}{\partial t^2} + \frac{\partial J}{\partial t} \quad (2.42)$$

We consider the characteristic value when there is loss in the medium. When we consider the incidence of the time-varying factor  $\exp(j\omega t)$ , Maxwell's Equation can be written as follows.

$$\text{rot}H = \epsilon\epsilon_0 \frac{\partial E}{\partial t} + \sigma \mathbf{E} = (j\omega\epsilon\epsilon_0 + \sigma)\mathbf{E} \quad (2.43)$$

In this case, the right-hand side of Equation 2.43 is considered to arise from the flux density  $\mathbf{D}$ .

$$\mathbf{D} = C\epsilon\epsilon_0 \mathbf{E}(\mathbf{r})\exp(j\omega t) \quad (2.44)$$

We derive the constant  $C = 1 - j\sigma/\omega\epsilon\epsilon_0$  from the equation above. Thus the electric flux density can be written as

$$\mathbf{D} = \dot{\epsilon}\epsilon_0 \mathbf{E} = \epsilon\epsilon_0(1 - j\tan\delta)\mathbf{E} \quad (2.45)$$

$$\dot{\epsilon} = \epsilon(1 - j\tan\delta) \quad (2.46)$$

$$\tan\delta = \frac{\sigma}{\omega\epsilon\epsilon_0} \quad (2.47)$$

The parameter in Eq. 2.47 is known as the loss tangent. At high frequencies, the contribution of the real part of  $\epsilon$  becomes larger, while at low frequencies, the contribution of the imaginary part becomes larger. In other words, it can be said that when an AC electric field is applied to a dielectric, a part of its energy is the ratio that becomes heat.

## 2.8 Skin effect

Skin effect is the tendency of an alternating current to flow mostly near the outer surface of an electrical conductor, such as copper plates. In many of the experiments in this study, millimeter waves are blocked by copper plates. The conductivity of the conductor  $\sigma$  increases, and the amplitude damping constant  $\alpha$  and the phase constant  $\beta$  can be estimated as below.

$$\alpha \approx \beta \approx \sqrt{\frac{\omega \mu \mu_0 \sigma}{2}} \quad (2.48)$$

This means that the attenuation of electromagnetic waves increases with increasing conductivity of  $\sigma$  and the electromagnetic wave attenuates exponentially. The depth  $\delta$  at which the amplitude of the electromagnetic wave at the surface is  $1/e$  is called the skin depth, which can be expressed as below.

$$\delta = \frac{1}{\alpha} = \sqrt{\frac{2}{\omega \mu \mu_0 \sigma}} \quad (2.49)$$

This indicates that the skin depth becomes shallower as the frequency of the electromagnetic wave increases and the conductivity increases. In this case, the current flows only near the surface of the copper plate, which is called the skin effect. The fact that current flows means that resistance exists, and the skin resistance is written as follows.

$$Re\{Z_W\} = \sqrt{\frac{\omega \mu \mu_0}{2}} = \frac{1}{\delta \sigma} \quad (2.50)$$

Therefore copper plates can be used to effectively block millimeter waves.

## 2.9 Snell's law

At the boundary surfaces of different media, reflection and refraction of electromagnetic waves occur. This is described by Snell's law. This law can be derived using Maxwell's equations and boundary conditions.

The boundary plane of the medium is the x-y plane, and the medium is uniform in the y direction within each region. The relative permittivity and relative permeability are  $\epsilon_1$  and  $\mu_1$  for the first medium, and  $\epsilon_2$  and  $\mu_2$  for the second medium. Let the complex permittivity in the presence of loss be  $i$  for each medium, so take values of 1 and 2, respectively.

$$\epsilon_i = \epsilon(1 - j \frac{\sigma_i}{\omega \epsilon_i \epsilon_0}) \quad (2.51)$$

Here  $\sigma$  is the conductivity,  $\omega$  is the angular frequency of the electromagnetic wave,  $\epsilon$  is the dielectric constant when there is no loss, and  $\epsilon_0$  is the dielectric constant of vacuum.

The specific permeability  $\mu$  is assumed to be a real number this time. Here the magnitude of the wavenumber of each medium is as follows as  $k$ .  $c$  is the speed of light in vacuum.

$$k_i = \frac{\omega\sqrt{\epsilon_i\mu_i}}{c} \quad (2.52)$$

Here we derive Snell's law using the TE wave as an example. For TE waves, the oscillation direction of the electric field is perpendicular to the surface, and there is no electric field component in the direction of propagation. Since the direction perpendicular to the surface is the  $y$ -axis, its electric field is  $E_y^i$  and can be written as follows:

$$E_y^i = A_{iS} \exp[j(\omega t - \mathbf{k}_i \cdot \mathbf{r})] \quad (2.53)$$

$A_{iS}$  is the electric field amplitude,  $\mathbf{k}_i$  is the wavenumber vector in the medium, and  $\mathbf{r}$  is the position vector to an arbitrary point on the wavefront. The subscript  $i$  has three states, where incident, transmitted, and reflected are denoted by i, t, and r, respectively.

## 2.10 Total Reflection

When an electromagnetic wave is incident on a sparse medium from a dense medium, the refraction angle reaches 90 degrees before the incident angle as the incident angle is gradually increased. This phenomenon in which the incident electromagnetic wave returns to the incident side after being reflected at the boundary surface without being transmitted is called total reflection.

The transmitted field components of the TE wave at total reflection can be written as follows.

$$E_y^t = \exp[-j(\sqrt{\epsilon_1\mu_1}k_0 \sin \theta_t)x] \exp\left(-\frac{z}{z_g}\right) \quad (2.54)$$

$$z_g = \frac{c}{\omega\sqrt{\epsilon_1\mu_1 \sin^2 \theta - \epsilon_2\mu_2}} \quad (2.55)$$

$z_g$  represents the depth of penetration of the electric field into the second medium, indicating that the electromagnetic wave is seeping slightly into the boundary surface. Even during total reflection, electromagnetic waves also slightly penetrate to the other side of the boundary. This component is called the evanescent wave. Along with the penetration of the electromagnetic field, the reflection point is also shifted. This shift is called the Guschenchen shift. This is important when using dielectric waveguides and optical fibers.

Electromagnetic waves do seep out slightly to the other side of the boundary plane, but it is important to note that the energy does not seep out. It is important to note that energy does not seep out. The sum of the amplitude reflection coefficients all add up to 1, and all energy is also reflected.

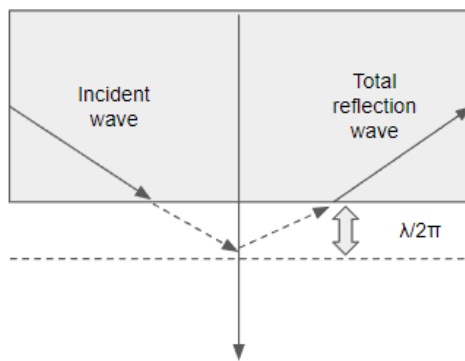


Fig. 2.10: Evanescence waves present in total internal reflection

## 2.11 Link budget

A link budget is an accounting of all of the power gains and losses that a communication signal experiences in a telecommunication system; from a transmitter, through a communication medium such as radio waves, cable, waveguide, or optical fiber, to the receiver. Link budget is controlled by three factors, which are communication distance, transmitted power, and antenna gain.

To calculate the link budget, we first need to calculate the EIRP (Equivalent Isotropically Radiated Power)[W], which is the sum of the output power of the transmitter, antenna gain, and cable loss, which can be written as follows:

$$EIRP = TP + Gain - Loss \quad (2.56)$$

EIRP and TP are short for received power and transmitted power, respectively. While EIRP and TP are in units of decibels-milliwatts, gain and loss are in units of decibels. TP is further determined by the cable loss and the transmitted power of the device itself. Here we omit some variables such as miscellaneous losses, which include polarization mismatch and fading margin.

For example, when the input power of the transmitter and the gain is -11 dBm and 5 dBi, respectively, the EIRP is -6 dBm. If the gain on the receiver antenna is 5dBi and the path loss is 49.3 dB, the received power on the receiver antenna can be calculated as:

$$P_r = EIRP - L_a + G_r = -50.3dBm \quad (2.57)$$

The table below summarizes the situation discussed above:

This indicates again the limitations of the millimeter wave in an open space. Millimeter waves with frequency of 28GHz have a loss of -49.3 dB just within 0.25 meters of communication distance.

Table 2.2: Table of all factors affecting the communication system

Factors	Values	Unit
Tx Power	-10	dBm
Tx Cable Loss	-1	dB
Tx ANT Gain	5	dBi
EIRP	-6	dBm
Distance	0.25	m
Air loss	-49.3	dBi
Rx ANT Gain	5	dBi
Rx Cable Loss	-1	dB
Rx Input	-51.3	dBm

## 2.12 S parameters

TODO: write here

## 2.13 Cutoff Frequency

A cutoff frequency, corner frequency, or break frequency is a boundary in a system's frequency response at which energy flowing through the system begins to be reduced rather than passing through. This means that the signals with a frequency above the cut-off frequency will travel through a waveguide and signals below this frequency will be attenuated.

Using the fact that the components of the wavenumber must satisfy the relationship:

$$k_x^2 + k_y^2 + k_z^2 = \omega^2 \mu \epsilon = \left( \frac{2\pi f}{c} \right)^2 \quad (2.58)$$

Assuming the situations are the same as in the equations 2.22 and 2.23, by plugging them in we get:

$$\left( \frac{m\pi}{a} \right)^2 + \left( \frac{n\pi}{b} \right)^2 + k_z^2 = k^2 = \left( \frac{2\pi f}{c} \right)^2 \quad (2.59)$$

$k_z^2 > 0$  is the necessary condition for propagation to occur. If this is true, then  $k_z$  is a real number, so that the field components will contain complex exponentials, which represent propagating waves. Otherwise when  $k_z^2 < 0$ ,  $k_z$  will be an imaginary number, in which case the complex exponential becomes a decaying real exponential. In this case, the fields will not propagate but instead quickly die out within the waveguide. Electromagnetic fields that die off instead of propagate are referred to as evanescent waves.

TODO add here <https://www.antenna-theory.com/tutorial/waveguides/waveguides3.php>

Cutoff frequency  $f_c$  in a rectangular waveguide can be calculated as follows, where  $a$  is the wall length, and  $\mu$  and  $\epsilon$  are the permeability and permittivity of the material that fill the waveguide, respectively.

$$f_c = \frac{1}{2a\sqrt{\mu\epsilon}} \quad (2.60)$$

In a circular waveguide with radius of  $a$ ,  $f_c$  could be written as

$$f_c = \frac{1.8412}{2\pi a\sqrt{\mu\epsilon}} \quad (2.61)$$

## 2.14 Usecases

This approach show the advantages in the following aspects compared to other communication mediums.

1. **Cost efficiency** Flexible dielectric waveguides are cheaper compared to SMA cables and horn antennas. The length and radius of the PTFE sticks can be also adjusted easily.
2. **Flexibility** Flexible dielectric waveguides can be bent flexibly, unlike horn antennas, which make them suitable in environments with less space.
3. **Low propagation loss** Compared to SMA cables, dielectric waveguides have less loss when propagating signals in the millimeter wave bands.

The high resolution beam from the dielectric waveguide enables users and devices to create an one to one connection with the access point. From the perspective of security, this eliminates the possibility of malicious devices spying on the electromagnetic signals emitted from the device.

This approach allows the users and their devices to create a secure connection in the physical layer. Numerous studies have been done on the software side to protect the data communicated between the device and the access point by using encryption algorithms, such as AES. Our approach is different from previous studies in the sense that secure communication zones are created in the physical world.

This approach can be used in offices where employees handle vital information that cannot be leaked, and in places such as ATMs, where customers often look up important information on their smartphones before making transactions from their bank accounts.

## 2.15 Two Dimensional Waveguide Sheets

## 2.16 Finite Element Boundary Integral Method

Exact numerical solutions of electromagnetic radiation and scattering problems including arbitrarily shaped conducting objects preferably rely on integral equations (IEs) being solved by the method of moments (MoM), usually employing Galerkin's method with triangular Rao-Wilton-Glisson (RWG) vector basis functions. For problems including arbitrarily shaped and inhomogeneous dielectric objects, the hybrid finite element—boundary integral (FEBI) method has been developed, where the fields in the interior region of the dielectric objects are formulated with the FE method and the fields in the exterior region with an IE. The two regions are coupled together at the boundaries of the objects via the field continuity conditions. In order to avoid interior resonances and for improved convergence within the iterative solver, the combined field integral equation (CFIE) is used, which is a linear combination of the electric field integral equation (EFIE) and the magnetic field integral equation (MFIE). The finite element boundary integral method combines the finite element method (FEM) and the surface integral equation embodied in the extended boundary condition method (EBCM).

The theory of the extended boundary condition method is well known and only the equations which are required for the extension of the technique to the inhomogeneous problem will be given here. Consider a scatterer illuminated by a plane wave. The incident field  $\bar{E}_i$  and the scattered field  $\bar{E}_s$ , can be expanded in the spherical vector harmonics  $\bar{M}$  and  $\bar{N}$ .

$$\bar{E}_i = \sum_{\nu} D_{\nu} [a_{\nu} \bar{M}_{\nu}^1(k_0 \bar{r}) + b_{\nu} \bar{N}_{\nu}^1(k_0 \bar{r})] \quad (2.62)$$

$$\bar{E}_s = \sum_{\nu} D_{\nu} [f_{\nu} \bar{M}_{\nu}^4(k_0 \bar{r}) + g_{\nu} \bar{N}_{\nu}^4(k_0 \bar{r})] \quad (2.63)$$

The  $a_{\nu}$  and  $b_{\nu}$  coefficients are known, while  $f_{\nu}$  and  $g_{\nu}$ , are initially unknown.  $D_{\nu}$  is a normalization constant,  $\nu$  is a combined index incorporating the three spherical harmonic indices. and  $k_0$  is the free space wave number.

TODO: write rest <https://core.ac.uk/download/pdf/36739115.pdf>

### 2.16.1 Boundary Integral Equation Methods

We can reformulate boundary value problems for partial differential equations in a domain as integral equations on the boundary of that domain. Boundary integral equation methods refer to the numerical solution of these integral equations. Since we only solve a problem on the boundary, there is an overall reduction in dimension by one. Also because of its meshless characteristics, it can compute solutions in complicated domains. In some situations, it is easier to integrate than to differentiate. The difference between partial differential equations and integral equations is that numerical solution of partial differential

equations yield sparse matrices, while numerical solutions of boundary integral equations yield dense matrices.

## 2.17 Radiation Conditions

When the outer boundary of a domain recedes to infinity, the domain is called unbounded or open. A condition must be specified at this outer boundary to obtain a unique solution for this problem. Such a condition is referred to as a radiation condition.

Assuming that all sources and objects are immersed in free space and located within a finite distance from the origin of a coordinate system, the electric and magnetic fields are required to satisfy:

$$\lim_{r \rightarrow \infty} \left[ \nabla \times \begin{pmatrix} \mathbf{E} \\ \mathbf{H} \end{pmatrix} + jk_0 \hat{r} \times \begin{pmatrix} \mathbf{E} \\ \mathbf{H} \end{pmatrix} \right] = 0 \quad (2.64)$$

where  $r = \sqrt{x^2 + y^2 + z^2}$ . This is referred to as the Sommerfeld radiation condition for general three-dimensional fields, and is exactly valid at infinity. In numerical analysis, it is often desirable to reduce the size of a computational domain by using a finite boundary to truncate the infinite domain. When applied at such a finite boundary, 2.64 can be regarded as the lowest-order radiation condition with limited accuracy. Better accuracy can be achieved by developing higher-order conditions.

## 2.18 Huygens' principle

Huygens' principle provides expressions to calculate the fields everywhere based on knowledge of the fields surrounding an object. Consider a surface  $S$  enclosing the source of radiation and any other objects so that the infinite space exterior to the surface is homogeneous (TODO ref fig). If the fields on the surface are known, the fields outside the surface are given by:

$$\mathbf{E}(\mathbf{r}) = \oint_S -j\omega\mu[\hat{n}' \times \mathbf{H}(\mathbf{r}')]G_0(\mathbf{r}, \mathbf{r}') + [n' \cdot \mathbf{E}(\mathbf{r}')] \nabla' G_0(\mathbf{r}, \mathbf{r}') + [\hat{n}' \times \mathbf{E}(\mathbf{r}')] \times \nabla' G_0(\mathbf{r}, \mathbf{r}') dS' \quad (2.65)$$

TODO: keep writing

## 2.19 Variational Method

A typical boundary-value problem can be defined by a governing differential equation in a domain  $\Omega$ , and the boundary conditions on the boundary  $\Gamma$  that encloses the domain.

$$L\phi = f \quad (2.66)$$

Here  $L$  is a differential operator,  $f$  is the excitation function, and  $\phi$  is the unknown quantity. Poisson equation is an example of a governing differential equation in electromagnetics and Dirichlet condition is an example of a boundary condition.

### 2.19.1 The Ritz Method

The operator  $L$  is self-adjoint when it satisfies the following condition:

$$\langle L\phi, \psi \rangle = \langle \phi, L\psi \rangle \quad (2.67)$$

An example of a self-adjoint operator is  $i \frac{d}{dx}$ . (A simple instance of this can be calculated by using the operator on  $\phi = e^{ix}$ . Check the following  $[L\phi]\phi^* = \phi[L^*\phi^*]$  is satisfied) To obtain the solution, we must add another condition that the operator  $L$  is positive definite, that is:

$$\langle L\phi, \phi \rangle = \begin{cases} > 0 & \phi \neq 0 \\ = 0 & \phi = 0 \end{cases} \quad (2.68)$$

And the solution to Equation 2.67 can be obtained by minimizing the functional

$$F(\tilde{\phi}) = \frac{1}{2} \langle L\tilde{\phi}, \tilde{\phi} \rangle - \langle \tilde{\phi}, f \rangle - \langle f, \tilde{\phi} \rangle \quad (2.69)$$

Here  $\tilde{\phi}$  represents a trial function. To prove this variational principle, we first need to show the differential equation is the necessary consequence when the functional  $F$  is stationary ( $\delta F = 0$ ). We also must prove that the stationary point is at the minimum of the functional  $F$ , which is equivalent to proving that  $\delta(\delta F) > 0$ . Taking the variation again,

$$\delta F = \frac{1}{2} \langle L\delta\phi, \phi \rangle + \frac{1}{2} \langle L\phi, \delta\phi \rangle - \frac{1}{2} \langle \delta\phi, f \rangle - \frac{1}{2} \langle f, \delta\phi \rangle \quad (2.70)$$

and using the condition is that  $L$  is self-adjoint,

$$\frac{1}{2} \langle L\delta\phi, \phi \rangle = \frac{1}{2} \langle L\phi, \delta\phi \rangle \quad (2.71)$$

allows us to simplify the equation as follows:

$$\delta F = \frac{1}{2} \langle \delta\phi, L\phi - f \rangle - \frac{1}{2} \langle L\phi - f, \delta\phi \rangle \quad (2.72)$$

The definition of the inner product lets us have

$$\delta F = \frac{1}{2} \langle \delta\phi, L\phi - f \rangle - \frac{1}{2} \langle \delta\phi, L\phi - f \rangle^* = Re \langle \delta\phi, L\phi - f \rangle \quad (2.73)$$

Here  $Re$  denotes the real part of the equation it encloses. Imposing the stationary requirement  $\delta F = 0$ , we obtain

$$\operatorname{Re}\langle \delta\phi, L\phi - f \rangle = \operatorname{Re}\left\langle \int_{\Omega} \delta\phi (L\phi - f)^* d\Omega \right\rangle = 0 \quad (2.74)$$

$\delta\phi = 0$  can be ignored since it is an arbitrary variation, and from  $L\phi - f = 0$ , the first point is proved.

The second point can be considered by taking the first variation of  $\delta F$  once more. This results in:

$$\delta(\delta F) = \delta F(\phi + \delta\phi) - \delta F(\phi) = \operatorname{Re}\langle \delta\phi, L\delta\phi \rangle \quad (2.75)$$

For a nontrivial (non-zero)  $\delta\phi$ , using the positive definite condition, we can conclude that  $\delta(\delta F) > 0$ . Rephrasing this, when  $L > 0$  and  $\delta\phi > 0$ , the result of Equation 2.75 is greater than 0. Therefore the stationary point is indeed at the minimum of  $F$ .

## 2.19.2 Galerkin's Method

### 2.19.3 A Simple example

Here we look at a simple boundary-value problem and solve it using both the Ritz and Galerkin methods. The problem is about the determination of the static potential  $\phi$  between two infinite parallel plates. One plate is located at  $x = 0$  with  $\phi = 0$  and the other at  $x = 1$  with  $\phi = 1$ . The space between is filled with a medium having a constant permittivity of  $\epsilon$  F/m and a varying electric charge density of  $\rho(x) = -(x + 1)\epsilon$  C/m<sup>3</sup>.

The Poisson equation can be applied to this problem as follows (we do not take off the minus at the both sides of the equation for simplicity):

$$-\frac{d^2\phi}{dx^2}\epsilon = -(x + 1)\epsilon \quad (2.76)$$

The boundary conditions are given as:

$$\phi|_{x=0} = 0 \quad (2.77)$$

$$\phi|_{x=1} = 1 \quad (2.78)$$

This is simply a second-order differential equation, and can be solved easily by integrating the equation twice. Here we assume we do not know the exact solution and use the Ritz and Galerkin methods to find it.

#### Solution via the Ritz Method

In the Ritz method, a functional is defined where the minimum of the functional corresponds to the differential equation under the given boundary conditions. From eq. 2.67,

## 2.20. SUMMARY

---

the differential operator  $L$  is  $-\frac{d^2}{dx^2}$  (which is a self-adjoint operator and satisfies the conditions to be used for the Ritz method), and  $-(x + 1)$  is the forcing function. Plugging them into the equation 2.66, we get:

$$F(\tilde{\phi}) = \frac{1}{2} \int_0^1 \left(-\frac{d^2}{dx^2}\phi\right)\phi^* dx + \frac{1}{2} \int_0^1 \tilde{\phi}(x + 1)dx + \frac{1}{2} \int_0^1 (x + 1)\tilde{\phi}^* dx \quad (2.79)$$

Since the problem here does not contain imaginary numbers, we can say  $\tilde{\phi} = \tilde{\phi}^*$ . Also, since  $i\frac{d}{dx}$  is also a self adjoint operator,

$$\left(-\frac{d^2}{dx^2}\tilde{\phi}\right)\tilde{\phi}^* = (i\frac{d}{dx}\tilde{\phi})(-i\frac{d}{dx}\tilde{\phi}^*) = (i\frac{d}{dx}\tilde{\phi})(i\frac{d}{dx}\tilde{\phi})^* = \left|\left(i\frac{d}{dx}\tilde{\phi}\right)\right|^2 \quad (2.80)$$

Therefore the functional equation can be simplified as:

$$F(\tilde{\phi}) = \frac{1}{2} \int_0^1 \left(\frac{d}{dx}\tilde{\phi}\right)^2 dx + \int_0^1 \tilde{\phi}(x + 1)dx \quad (2.81)$$

Here we use polynomials as one of the candidate trial functions:

$$\tilde{\phi}(x) = c_1 + c_2x + c_3x^2 + c_4x^3 \quad (2.82)$$

From the boundary conditions, the conditions  $c_1 = 0$ ,  $c_2 = 1 - c_3 - c_4$  are obtained. This reduces the current function to

$$\tilde{\phi}(x) = x + c_3(x^2 - x) + c_4(x^3 - x) \quad (2.83)$$

Substituting the above equation to 2.81, the following derivatives are obtained:

$$\frac{\partial F}{\partial c_3} = \frac{1}{3}c_3 + \frac{1}{2}c_4 - \frac{1}{4} \quad (2.84)$$

$$\frac{\partial F}{\partial c_4} = \frac{1}{2}c_3 + \frac{4}{5}c_4 - \frac{23}{60} \quad (2.85)$$

By setting these derivatives to zero,  $c_3 = \frac{1}{2}$  and  $c_4 = \frac{1}{6}$  can be computed. Here the trial functions employed were capable of representing the exact function, but this usually is impossible. In most situations, only approximate solutions can be achieved.

## 2.20 Summary

In this section we first reviewed Maxwell's equations, and Hugens' principle for calculating exterior fields from the field on a closed surface.

TODO: insert figure

## 2.21 Rod Antennas

## 2.22 Tools to Use

### 2.22.1 Vector network analyzers

TODO

### 2.22.2 Connectors

TODO

### 2.22.3 MZ-mmCon1

MZ-mmCon1, shown in Figure 2.11, enables converting baseband signals of the 5 MHz to 6 GHz range up to the 27 GHz to 43 GHz range, and vice versa. It contains a 32 bit STM32F microcontroller containing both 12 bit analog to digital, digital to analog converters. The microcontroller also employs a wave table of maximum 4096 words with 2 channels, which can create and send constant wave signals. The microcontroller can also create arbitrary wave signals from data written in the flash memory. The device alone can produce constant wave and narrow band wave signals of under 100 kHz, and can modulate, demodulate, send, and receive millimeter wave signals. Upon receiving millimeter waves, the signal is demodulated and the baseband signal is converted to a digital signal, which can be analyzed on the computer by applying Fast Fourier Transformation (FFT). Figure 2.13 shows the FFT result visualized on the installed software.

### 2.22.4 MZ-mmAnt1

The MZ-mmAnt1 is a patch antenna designed for propagation of 28 GHz millimeter waves, with an antenna gain of roughly 5 dB. Using a SMPM to K connector adapter, the antenna can be hooked to the band pass filter and the up / down converter. The antenna can also be hooked up to a tripod by using the hole dug into the bottom of the structure.

### 2.22.5 Shield Box

A brass shield box was designed to emit the 60 GHz millimeter waves in a straightforward direction and prevent the waves from leaking out to other directions, as shown in Figure 2.16.

The VR-WH1 sender device was placed inside the box, as shown in 2.17.

## 2.22. TOOLS TO USE

---

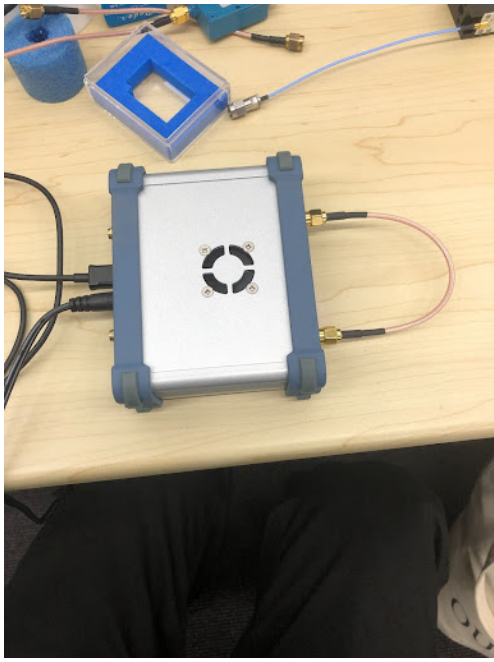


Fig. 2.11: MZ-mmcon1 in loopback mode



Fig. 2.12: Adalm Pluto

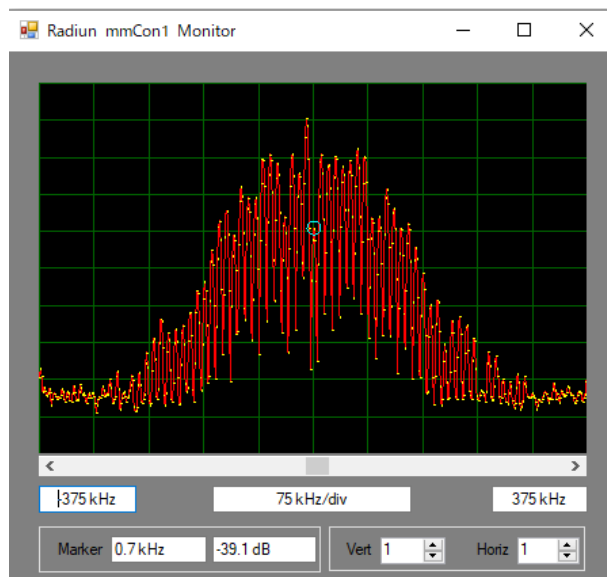


Fig. 2.13: FFT visualization on the software

## 2.22. TOOLS TO USE

---



Fig. 2.14: mz-mmAnt1

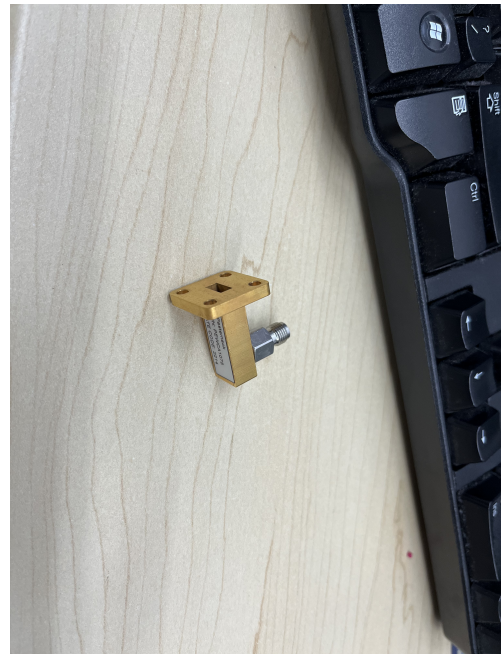


Fig. 2.15: Waveguide to Coax Adapter



Fig. 2.16: Shield Box

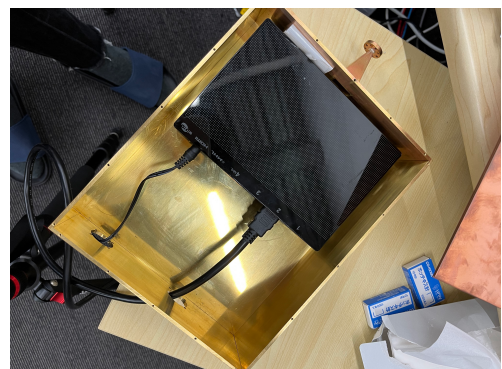


Fig. 2.17: VR-WH1 placed inside shield box

### 2.22.6 Adalm Pluto

The ADALM-PLUTO Active Learning Module (PlutoSDR) is a tool available from Analog Devices Inc. (ADI) that can be used to simulate fundamental features of software-defined radio (SDR) or radio frequency (RF). The Communications Toolbox Support Package for Analog Devices ADALM-PLUTO Radio (PlutoSDR) enables the programmer to use MATLAB and Simulink to prototype, verify, and test practical wireless systems.

Here, the QPSK transmitter was implemented on Pluto to calculate the bit error rate in a 28GHz system. Bit error rate can be calculated as follows:

$$BER = \frac{\text{Number of error bits}}{\text{Number of total bits}} \quad (2.86)$$

### 2.22.7 Waveguide to Coax Adapter

For the 28 GHz system, we used the WR-28 UG-599/U square cover flange to 2.92mm female waveguide to coax adapter, which operates from 26.5 GHz to 40 GHz. The product ID of this adapter is PEWCA1078. This adapter offers a WR-28 waveguide interface size coupled with a precision tolerance UG-599/U flange. The PEWCA1078 is constructed of copper and plated in gold to ensure durability and repeatable RF performance.

### 2.22.8 Spectrum Analyzer

The Anritsu MS2762A spectrum analyzer was used for the 28 GHz system. Utilizing Anritsu's patented nonlinear transmission line (NLTL) technology, it provides continuous coverage from 6 GHz to 170 GHz, with displayed average noise level (DANL) of -141/-136/-129/-122 dBm to 90/110/145/170 GHz, respectively. Powered by a USB type-C port, the spectrum can be analyzed on a Windows PC using the software provided by Anritsu. As the MS2762A port only supports the 0.8 mm connector, the following adapters were used to convert it to a K connector port (shown in Figure 2.18).

- 33W.8F50 (0.8 mm to W)
- 34WFV50 (W to V)
- 34VFKF50A (V to K)

## 2.23 Communication Medium Used in Embedded Systems

### 2.23.1 UART

UART, or universal asynchronous receiver-transmitter, is one of the most used device-to-device communication protocols. When properly configured, UART can work with many

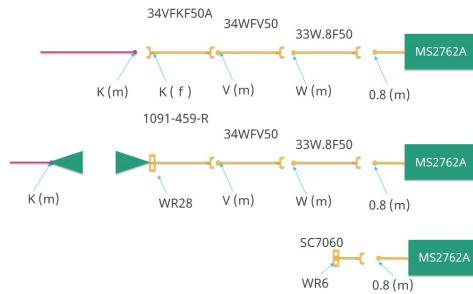


Fig. 2.18: Conversion of the port on MS2762A



Fig. 2.19: The mz-mmAnt1 hooked up to the MS2762A

different types of serial protocols that involve transmitting and receiving serial data. In serial communication, data is transferred bit by bit using a single line or wire. In two-way communication, two wires are used for successful serial data transfer. Depending on the application and system requirements, serial communications needs less circuitry and wires, which reduces the cost of implementation. Here we explain the fundamental principles when using UART, with a focus on packet transmission and standard frame protocol.

The image of the interface with data bus is shown in Figure 2.20.

The two signals of each UART device are named:

- Transmitter (Tx)
- Receiver (Rx)

The transmitting UART is connected to a controlling data bus that sends data in a parallel form. From this, the data will now be transmitted on the transmission line (wire) serially, bit by bit, to the receiving UART. This, in turn, will convert the serial data into parallel for the receiving device.

For UART and most serial communications, the baud rate needs to be set the same on both the transmitting and receiving device. The baud rate is the rate at which information is transferred to a communication channel. In the serial port context, the set baud rate will serve as the maximum number of bits per second to be transferred.

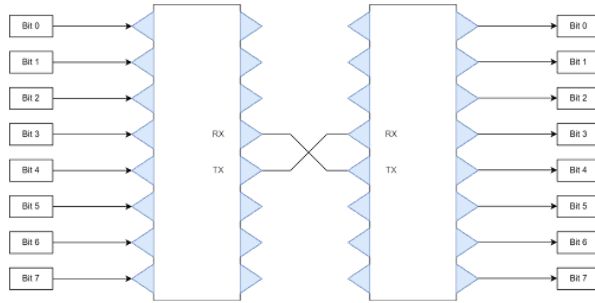


Fig. 2.20: UART with data bus



Fig. 2.21: UART packet

The UART interface does not use a clock signal to synchronize the transmitter and receiver devices; it transmits data asynchronously. Instead of a clock signal, the transmitter generates a bitstream based on its clock signal while the receiver is using its internal clock signal to sample the incoming data. The point of synchronization is managed by having the same baud rate on both devices. Failure to do so may affect the timing of sending and receiving data that can cause discrepancies during data handling. The allowable difference of baud rate is up to 10% before the timing of bits gets too far off. The image of the UART packet is shown in Figure 2.21:

### 2.23.2 SPI

Serial peripheral interface (SPI) is one of the most widely used interfaces between microcontroller and peripheral ICs such as sensors, ADCs, DACs, shift registers, SRAM, and others. SPI is a synchronous, full duplex main-subnode-based interface. The data from the main or the subnode is synchronized on the rising or falling clock edge. Both main and subnode can transmit data at the same time. The SPI interface can be either 3-wire or 4-wire. Here we focus on the popular 4-wire SPI interface.

4-wire SPI devices have four signals:

- Clock (SPI CLK, SCLK)
- Chip select (CS)
- main out, subnode in (MOSI)
- main in, subnode out (MISO)

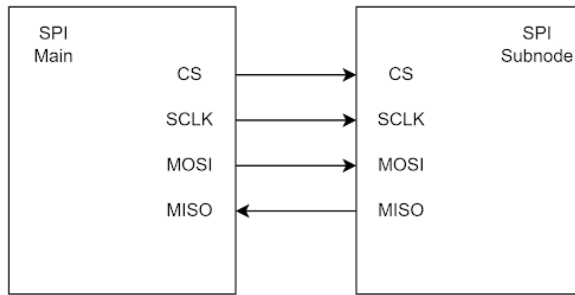


Fig. 2.22: SPI Communication

The device that generates the clock signal is called the main. Data transmitted between the main and the subnode is synchronized to the clock generated by the main. SPI devices support much higher clock frequencies compared to I<sup>2</sup>C interfaces. SPI interfaces can have only one main and can have one or multiple subnodes. The chip select signal from the main is used to select the subnode. This is normally an active low signal and is pulled high to disconnect the subnode from the SPI bus. When multiple subnodes are used, an individual chip select signal for each subnode is required from the main. MOSI and MISO are the data lines. MOSI transmits data from the main to the subnode and MISO transmits data from the subnode to the main.

To begin SPI communication, the main must send the clock signal and select the subnode by enabling the CS signal. Usually chip select is an active low signal; hence, the main must send a logic 0 on this signal to select the subnode. SPI is a full-duplex interface; both main and subnode can send data at the same time via the MOSI and MISO lines respectively. During SPI communication, the data is simultaneously transmitted (shifted out serially onto the MOSI/SDO bus) and received (the data on the bus (MISO/SDI) is sampled or read in).

## 2.24 Grating Couplers

## 2.25 Luneburg Lens

A Luneburg lens is a spherically symmetric gradient-index lens, shown in Figure 2.23. A typical Luneburg lens's refractive index  $n$  decreases radially from the center to the outer surface. They can be made for use with electromagnetic radiation from visible light to radio waves.

Each point on the surface of an ideal Luneburg lens is the focal point for parallel radiation incident on the opposite side. Ideally, the dielectric constant  $\epsilon_r$  of the material composing the lens falls from 2 at its center to 1 at its surface (or equivalently, the refractive index  $n$  falls from  $\sqrt{2}$  to 1), derived from the equation below:

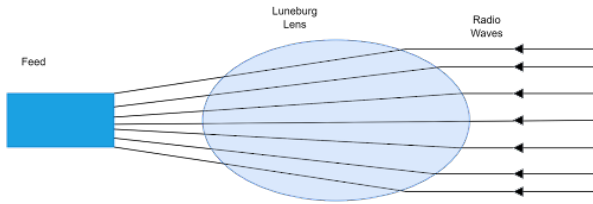


Fig. 2.23: Luneburg lens

$$n = \sqrt{\epsilon_r} = \sqrt{2 - \left(\frac{r}{R}\right)^2} \quad (2.87)$$

Here  $R$  is the radius of the lens. Because the refractive index at the surface is the same as that of the surrounding medium, no reflection occurs at the surface. Within the lens, the paths of the rays are arcs of ellipses.

### 2.25.1 Uses in a microwave antenna

A Luneburg lens can be used as the basis of a high-gain radio antenna. This antenna is comparable to a dish antenna, but uses the lens rather than a parabolic reflector as the main focusing element. As with the dish antenna, a feed to the receiver or from the transmitter is placed at the focus, the feed typically consisting of a horn antenna. The phase centre of the feed horn must coincide with the point of focus, but since the phase centre is invariably somewhat inside the mouth of the horn, it cannot be brought right up against the surface of the lens. Consequently it is necessary to use a variety of Luneburg lens that focuses somewhat beyond its surface, rather than the classic lens with the focus lying on the surface. A variation on the Luneburg lens antenna is the hemispherical Luneburg lens antenna or Luneburg reflector antenna. This uses just one hemisphere of a Luneburg lens, with the cut surface of the sphere resting on a reflecting metal ground plane.

We apply the lens in our millimeter wave antenna setup to realize an antenna with higher resolution.

## 2.26 Qualitative Analysis

The authors constructed a 60GHz mmWave system to qualitatively analyze the characteristics of the PTFE waveguide. VR-WH1, a wireless HDMI transmission unit manufactured by Sharp, was used. Video was first streamed on a PC and transmitted via HDMI to the sender unit. The sender unit is enclosed in a brass box with a horn antenna attached to the front. The PTFE waveguide is attached to the horn antenna, which the authors held with their hands to control its beam emission direction. The receiver was placed a meter



Fig. 2.24: Video does not play (data is not received) when the waveguide is not pointed to the receiver

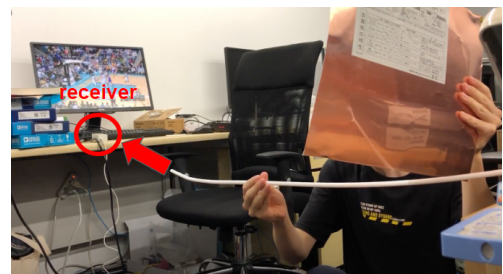


Fig. 2.25: Video plays when the waveguide is pointed to the receiver

away from the waveguide tip, and the receiver was connected to an external monitor via HDMI. The authors also held a copper board between the sender and the receiver just in case of wave leakage.

When using the 60GHz mmWave system, the authors discovered that the PTFE waveguide emits a sharp beam from its tip, as shown in Figures 2.24 and 2.25. The video does not play (data is not received on the receiver) when the waveguide is not pointed to the receiver, and vice versa when pointed.

TODO: add sharpened PTFE waveguide analysis.

## 2.27 Quantitative Analysis

### 2.27.1 Spectrum Results

### 2.27.2 Directivity Results

Working with NTT Docomo, the radiation patterns of the PTFE rod antenna were analyzed. The employed PTFE rod antenna had a diameter of 10 millimeters with a length of 20 centimeters. A PTFE rod antenna and the horn antenna were placed in an anechoic chamber with 1.2 meters in between.

The rod antenna was placed on a spinning platform , as shown in Fig. 2.28 and 2.29. The PTFE rod antenna and the platform rotate in the anechoic chamber with the tip of the PTFE rod antenna at the center of the rotation.

The results are shown in Figures 2.30 and 2.31. The half power beamwidth was at around 20 degrees for both vertical and horizontal radiation patterns, and no significant difference was seen across all of the frequencies. There is a slight distortion in the data due to the PTFE rod antenna's slight change in its orientation while spinning.

## 2.27. QUANTITATIVE ANALYSIS

---



Fig. 2.26: PTFE rod antenna with a diameter of 10 mm and length of 20 cm

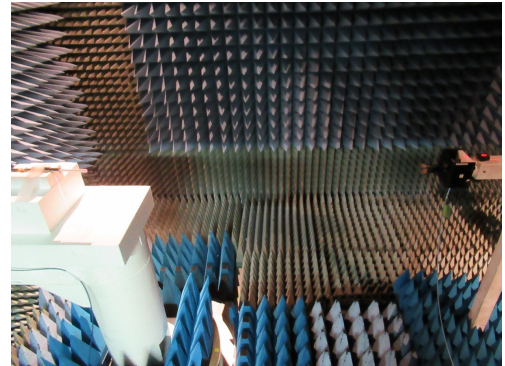


Fig. 2.27: Placement of antenna in anechoic chamber

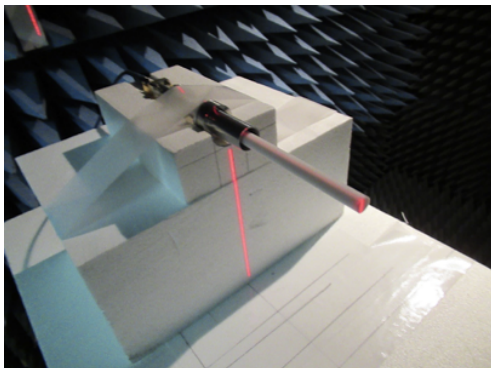


Fig. 2.28: PTFE rod antenna in anechoic chamber

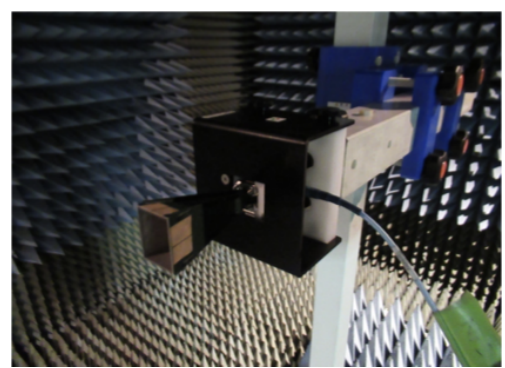


Fig. 2.29: Horn antenna in anechoic chamber

## 2.27. QUANTITATIVE ANALYSIS

---

Comparison of Radiation Patterns in the Vertical Field from 27 GHz to 29 GHz

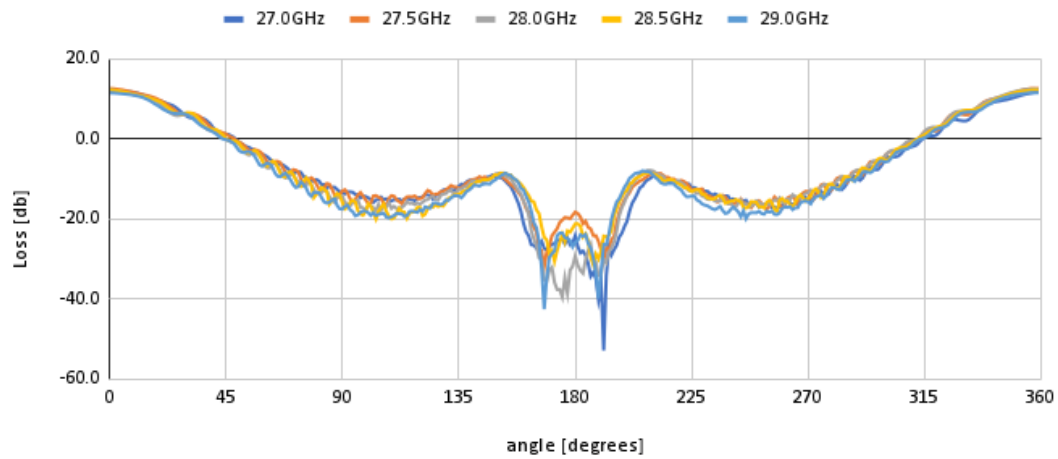


Fig. 2.30: Vertical Radiation Pattern

Comparison of Radiation Patterns in the Horizontal Field from 27 GHz to 29 GHz

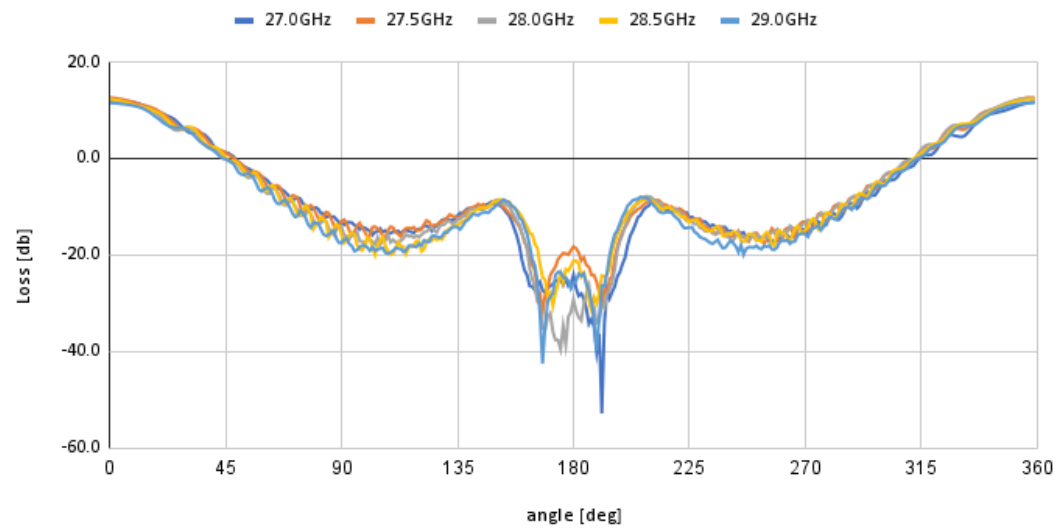


Fig. 2.31: Horizontal Radiation Pattern

# Chapter 3

## PTFE Rod Antenna

### 3.1 PTFE Rod Antenna Realization

### 3.2 Simulation Using HFSS

#### 3.2.1 About the simulation conditions

Here we discuss the simulation conditions used in HFSS. As shown in Figure 3.1, HFSS with Hybrid and Arrays was employed for the solution type. By choosing network analysis, HFSS solves the design by exciting the ports individually and loading the remaining ports by matched characteristic impedances. The modal option enables HFSS to use electromagnetic power to solve the simulation problem.

A hybrid region is defined to enclose the model, and the type is specified as FE-BI (finite element boundary integral), as seen in Figure 3.2.

Two modes were designed for the wave port to excite the HFSS models. Both of them have integration lines defined, and modes are aligned analytically using the coordinate system. The two vectors representing the integration lines span the diameter of the wave port, and are placed in perpendicular fashion (Figure 3.3).

We chose the 58 GHz to 60 GHz for the solution setup of the simulation, with a step size of 1 GHz (Figure 3.4).

#### 3.2.2 About the models

The models were all placed so that their radiation patterns were visualized on the x-y plane.

### 3.2. SIMULATION USING HFSS

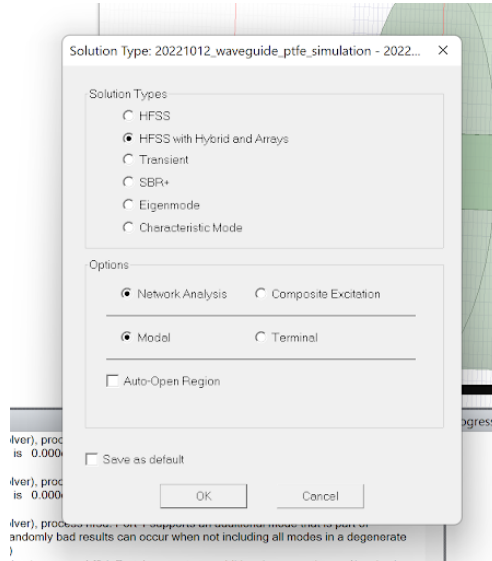


Fig. 3.1: Solution Type for HFSS

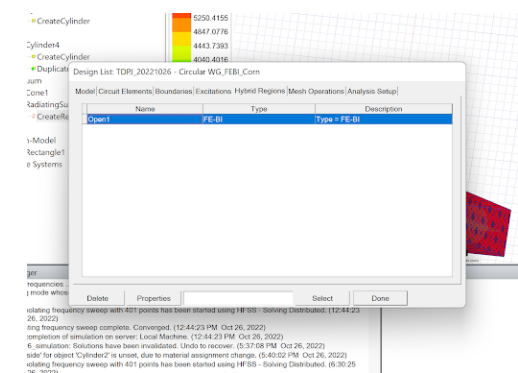


Fig. 3.2: Region Specification for HFSS

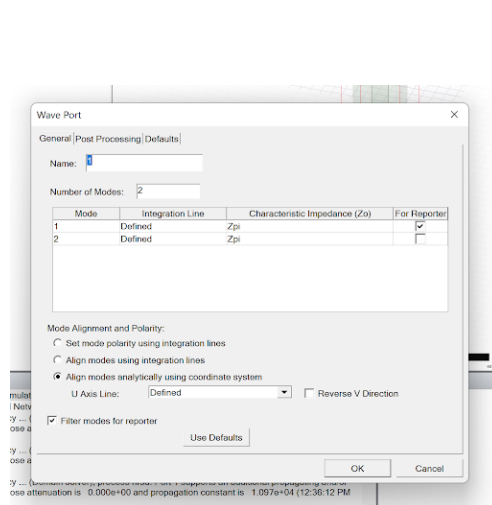


Fig. 3.3: Waveport Models for HFSS

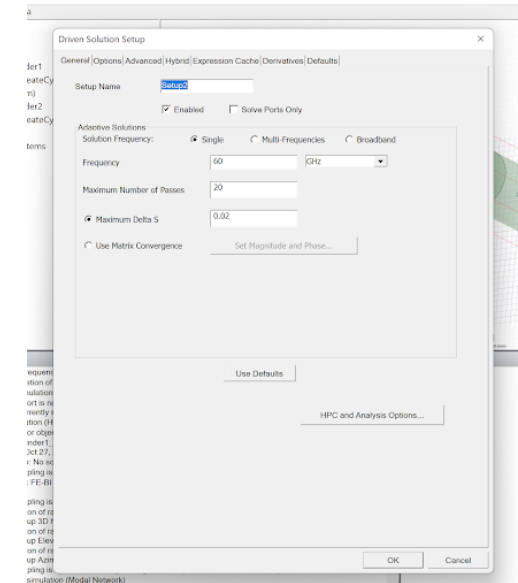


Fig. 3.4: Solution Setup for HFSS

### 3.2. SIMULATION USING HFSS

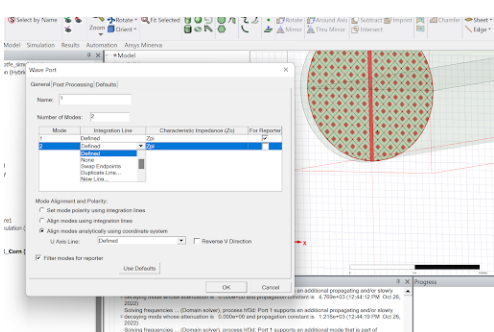


Fig. 3.5: Integration Line for HFSS

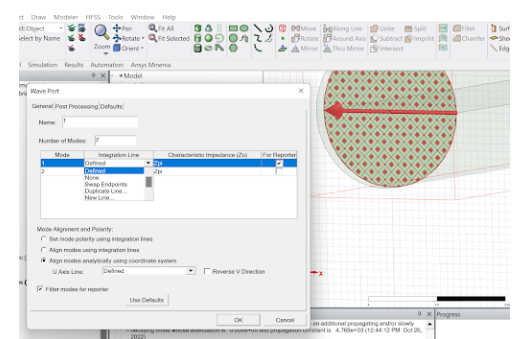


Fig. 3.6: Integration Line for HFSS

# Chapter 4

## Conclusion

In this paper, we presented a new method for communicating in a NLOS environment.

We can draw the following conclusions based on the antenna design process, simulation results and testing results.

TODO

# Chapter 5

## Future Work

In this paper, rod-like antennas were introduced to realize a high resolution communication system. Sheet-like antennas, where a dielectric sheet is used for propagating millimeter waves, were not considered in this paper and could be explored in future studies.

TODO

# Bibliography

- [1] INC. NTT DOCOMO. Docomo 6g white paper. 2014.
- [2] Shanzhi Chen, Shaohui Sun, Guixian Xu, Xin Su, and Yuemin Cai. Beam-space multiplexing: Practice, theory, and trends-from 4g td-lte, 5g, to 6g and beyond, 2020.
- [3] Kunihiro Kawai, Takuma Takada, Atsushi Fukuda, Hiroshi Okazaki, and Shoichi Narahashi. A new area formation approach for millimeter wave communication systems employing a dielectric waveguide. In *2015 European Microwave Conference (EuMC)*, pp. 1088–1091, 2015.
- [4] Atsushi Fukuda, Kunihiro Kawai, Hiroshi Okazaki, and Yasunori Suzuki. Experimental study of leaky-wave antenna employing bent dielectric waveguide for millimeter wave communication. In *2020 IEEE International Symposium on Radio-Frequency Integration Technology (RFIT)*, pp. 199–201, 2020.
- [5] Xiaofeng Lu, Fletcher Wicker, Pietro Lio, and Don Towsley. Security estimation model with directional antennas. pp. 1 – 6, 2008.